EXTRA SPINDLE POLES (Separase) controls anisotropic cell expansion in Norway spruce (*Picea abies*) embryos independently from its role in anaphase progression

Panagiotis N. Moschou[1], Eugene I. Savenkov[1*], Elena A. Minina[1,2*], Kazutake Fukada[1*], Salim Hossain Reza[1,2], Emilio Gutierrez-Beltran[1,2], Victoria Sanchez-Vera[1], Maria F. Suarez[3], Patrick J. Hussey[4], Andrei P. Smertenko[5,6] and Peter V. Bozhkov[1,2]

[1]Department of Plant Biology, Uppsala BioCenter, Swedish University of Agricultural Sciences and Linnean Center for Plant Biology, PO Box 7080, SE-75007 Uppsala, Sweden [2]Department of Chemistry and Biotechnology, Uppsala BioCenter, Swedish University of Agricultural Sciences and Linnean Center for Plant Biology, PO Box 7015, SE-75007 Uppsala, Sweden [3]Departamento de Biologia Molecular y Bioquimica, Facultad de Ciencias, Universidad de Malaga, 290071 Malaga, Spain [4]The Integrative Cell Biology Laboratory, School of Biological and Biomedical Sciences, University of Durham, Durham DH1 3LE, England, UK [5]Institute of Biological Chemistry, Washington State University, Pullman, WA 99164, USA [6]Institute for Global Food Security, Queen's University Belfast, 18-30 Malone Road, 13 Belfast, BT9 5BN, UK

*These authors contributed equally to this work

Corresponding author: Panagiotis N Moschou panagiotis.moschou@slu.se Tel: +46 700780553

Word count: 5,147, Total; Introduction 627; Material and Methods 1,400; Results 1,988; Discussion 1,132 (21%); Figures 7; Supporting Information: Figures 6, Tables 1, Methods 1, Files 1.

Summary

- The caspase-related protease separase (*EXTRA SPINDLE POLES*) plays a major role in chromatid disjunction and cell expansion in *Arabidopsis thaliana*. Whether the expansion phenotypes are linked to defects in cell division in Arabidopsis *ESP* mutants remains elusive.
- Here we present the identification, cloning and characterization of the gymnosperm Norway spruce (*Picea abies*) Pa *ESP*. We used *P. abies* somatic embryo system and a combination of reverse genetics and microscopy to explore the roles of Pa *ESP* during embryogenesis in gymnosperms.
- Pa *ESP* is expressed in the proliferating embryonal mass, while it is absent in the suspensor cells. Pa ESP associates with kinetochore microtubules in metaphase and then with anaphase spindle midzone. During cytokinesis it localizes on the phragmoplast microtubules and on the cell plate. Pa ESP deficiency perturbs anisotropic expansion and reduces the size of the stem cell niche in cotyledonary embryos. These functions of Pa ESP are independent of its role in chromatid disjunction.
- Our data demonstrate that ESP functions are evolutionary conserved in gymnosperms and angiosperms, and Pa ESP controls embryo development and cell expansion through mechanisms other than segregation of sister chromatids.

Keywords: embryogenesis, cell cycle, microtubules, proteases, separase, spruce

Introduction

Embryonic pattern formation in seed plants involves the establishment of apical-basal and radial polarities resulting in the formation of primary shoot and root meristems (Mayer *et al.,* 1991; Meinke, 1991; Ueda and Laux, 2012). Knowledge about plant embryogenesis has benefited from studies of embryo-defective mutants in the angiosperm model species *Arabidopsis thaliana* (Mayer *et al.,* 1991; Capron *et al.,* 2009; Kanei *et al.,* 2012; Wendrich and Weijers, 2013). However, our understanding of the molecular mechanisms underlying embryogenesis remains limited, owing to the restricted accessibility of zygotic embryos during early developmental stages. Somatic embryogenesis represents a valuable model for studying regulation of embryogenesis as it allows synchronized production of a large number of embryos at specific developmental stage and their life imaging (Pennell *et al.,* 1992; von Arnold *et al.,* 2002; Smertenko and Bozhkov, 2014).

Early embryogenesis in *Arabidopsis* proceeds through highly regular cell division patterns, starting with an asymmetric first division of the zygote, which gives rise to a smaller apical cell and a larger basal cell. The basal cell divides transversely to form a single file of suspensor cells and a hypophysis cell, while the apical cell undergoes several rounds of divisions to give rise to a globular embryo. This stage is followed by the establishment of bilateral symmetry and differentiation of two cotyledons. In most gymnosperms, e.g. Norway spruce (*Picea abies*), the zygote undergoes several rounds of karyokinesis without cytokinesis (free nuclear stage), followed by cellularization and formation of the lowest and the upper cell tiers (Singh, 1978). The lowest tier will form the embryonal mass (gymnosperm equivalent of embryo proper), while the upper tier will form the first layer of suspensor. A fully developed suspensor in spruce embryos is composed of several layers of elongated cells. Unlike *Arabidopsis*, spruce embryos form a crown of multiple cotyledons with radial symmetry surrounding the shoot apical meristem (Singh, 1978). Despite morphological differences in the embryo patterning in different plant lineages, the core regulatory network appears to be conserved (reviewed in Smertenko and Bozhkov, 2014).

Previous studies highlighted the importance of proteases in plant embryogenesis and other developmental processes (van der Hoorn, 2008). For example, in *Arabidopsis* a subtilisin-like serine protease ALE1 is required for cuticle formation in the protoderm (Tanaka *et al.,* 2001) and phytocalpain DEK1 is essential for embryogenic cell fate determination (Johnson *et al.,* 2005). *DEK1* mutant embryos that develop beyond globular stage show aberrant cell division planes in

the suspensor and embryo proper (Johnson *et al.*, 2005; Lid *et al.*, 2005). In addition, early embryonic patterning in Norway spruce requires the activity of metacaspase mcII-Pa (Suarez *et al.*, 2004; Minina *et al.*, 2013). Knockdown of *mcII-Pa* suppresses differentiation of the suspensor and abrogates establishment of apical-basal polarity.

Separase (ESP, Extra Spindle Poles) is a caspase-related protease required for embryogenesis in *Arabidopsis* (Liu and Makaroff, 2006) and non-plant species (e.g. Bembenek *et al.*, 2010). Initially, ESP was identified as an evolutionary conserved protein that cleaves cohesin to enable disjunction of daughter chromatids during metaphase-to-anaphase transition (referred to as the canonical function of ESP; Ciosk *et al.*, 1998). A temperature sensitive mutant allele of *ESP* from Arabidopsis (At *ESP), rsw4* (*radially swollen 4*), exhibits a chromosome non-disjunction phenotype (Wu *et al.*, 2010). In addition, *rsw4* causes disorganization of the radial microtubule system in meiocytes (Yang *et al.*, 2011) and defects in anisotropic expansion of root cells associated with radial swelling (Wu *et al.*, 2010).

Previously, we examined the role of At ESP in cell polarity and found that At ESP controls microtubule-dependent trafficking that is essential for cell plate synthesis during cytokinesis (Moschou *et al.*, 2013). Here we report the identification and functional characterization of the gymnosperm Norway spruce (*Picea abies*) ESP homologue Pa ESP, and explore the phenotype of spruce embryos depleted of Pa ESP.

Materials and Methods

Plant Material and Growth Conditions

The Norway spruce WT embryogenic cell lines 95.88.22 and 95.61.21, and Pa *ESP*-RNAi lines were cultured as described previously (Filonova *et al.*, 2000). Embryonal masses were separated from the suspensors of seven-day-old embryos using surgical blades in droplets of culture medium under a binocular microscope.

Molecular Biology

Primers used in this study are listed in Supplemental Table 1. Full length cDNA of the Pa *ESP* was obtained by 5'- and 3'-RACE with the SMART RACE cDNA Amplification kit (Clontech) and Advantage® 2 PCR kit (Clontech) with primers designed from publically available sequences of expression sequence tags (http://congenie.org/). Amplified PCR products were cloned into pCR4Blunt-Topo (Invitrogen). The plasmid carrying *FLAG-PaESP* sequence was constructed by ligating 5'-FLAG-PaESP fragment digested with PacI and AatII with 3'-end fragment digested with AatII and Sse8783I into the PacI/Sse8783I-cleaved pAHC25.

The *FLAG-PaESP* plasmid was used as template to amplify two overlapping fragments using primers FWPaESPExp1topo-Se-R3 (5'-fragment) and RvPaESPEXPAscI-Se-F2 (3'-fragment). The overlapping region contained a ClaI restriction site. The 5'-fragment was introduced into pTOPO/D vector (Invitrogen) giving rise to the pTOPO/D-PaESP 3.0 kb. The pTOPO/D vector contains an AscI site, upstream of the *att*R2 site. The remaining part of Pa *ESP* was introduced by digesting the 3'-fragment by ClaI and AscI and ligating it into pTOPO/D-PaESP 3.0 kb digested with ClaI and AscI, thus producing pTOPO/D-PaESP 6.9 kb. The PaESP insert was subcloned into pGWB15 (3xHA-tagged) vector by gateway recombination reaction using LR enzyme.

A 2,423-bp long C-terminal fragment was amplified with primers Sep-C-terminus CHis-P, Sep-CHis-M1 and Sep-CHis-M2 from pTOPO/D-PaESP 6.9 kb and introduced into a modified pET11a vector (Quiagen). The pET11a vector was modified by introducing a part from the polylinker of pKOH122 digested with NdeI and BamHI (amplified by pKOH122-MCS-P and MCS-reverse-with-SacI).

For constructing Pa *ESP*-RNAi vector, two fragments were amplified using primers FWPaESPExp1topo, PaESPRNAiRV1EcoRI, and FwPaESPRNAiAscI, PaESPRNAiRV2EcoRI.

Primer PaESPRNAiRV2EcoRI anneals 400 bp downstream of the PaESPRNAiRV1EcoRI. This 400 bp region represents the loop between two arms of the hairpin. The first fragment was cloned in a pTOPO/D vector, which was subsequently digested with EcoRI and AscI and the second fragment was introduced by ligation producing the pTOPO/D-hpRNAiPaESP vector. The hairpin insert was subcloned into a pGWB2 vector (constitutive silencing; Nakagawa *et al.*, 2007) or the pMDC7 [LexA-VP16-ER (XVE) *β*-estradiol inducible promoter, which is derived from the pER8 vector and contains the estrogen receptor-based transactivator XVE; Brand *et al.*, 2006]. The resulting constructs pGWB2-hpRNAiPaESP or pMDC7- hpRNAiPaESP were transformed into *Agrobacterium tumefaciens* GV3101 by electroporation. All constructs were verified by sequencing.

Phylogenetic Analysis

Alignments of ESP sequences were performed in ClustalW. Unrooted trees were constructed using the neighbor-joining method (Saitou and Nei, 1987) using the yeast homologue as an out-group. Phylodendrogram was constructed using PAUP software (http://paup.csit.fsu.edu). The bootstrap analysis was performed with 2,000 repeats and branches with bootstrap values over 70% were retained.

Embryo Transformation and Transient Expression

Norway spruce embryogenic cultures were transformed by *Agrobacterium tumefaciens* GV3101. Agrobacteria were grown overnight in LB medium supplemented with 10 mM $MgCl_2$, 10 mM 2-(N-morpholino)ethanesulfonic acid (MES) pH 5.5, 40 μM acetosyringone, 50 μg mL^{-1} rifampicin and 50 μg mL^{-1} kanamycin. Agrobacteria were collected and incubated for 1 h in 10 mM $MgCl_2$, 10 mM MES pH 5.5, 150 μM acetosyringone at room temperature on the shaker (OD_{600} = 10). Ten milliliters of five-day-old spruce culture (cell line 95.88.22) were collected in a 50 mL tube and the supernatant was discarded. The spruce culture was co-incubated with 1 mL *Agrobacterium* in 10 mL of 10 mM $MgCl_2$, 10 mM MES pH 5.5, 150 μM acetosyringone for 8 h without shaking at 20°C in darkness. Excess liquid was removed, spruce cells were placed on three layers of sterile filter paper and the upper layer was transferred on half-strength LP medium (Filonova *et al.*, 2008). After 48 h filter paper was transferred onto half-strength LP medium supplemented with 250 μg mL^{-1} cefotaxime (Duchefa), and after additional seven days onto the same medium with addition

of 15 μg mL^{-1} hygromycin B (Duchefa). Filters were transferred onto fresh medium once a week for consecutive six weeks. Subsequently, cell colonies were transferred onto the medium without filter papers, and grown in the presence of 250 μg mL^{-1} cefotaxime, 400 μg mL^{-1} timentin (Duchefa) and 15 μg mL^{-1} hygromycin B. After colonies were grown to approximately 2 cm in diameter, suspension cultures were established in half-strength LP without selection agents.

For transient expression of Pa *ESP*-RNAi, Norway spruce embryogenic cultures were transformed by *Agrobacterium tumefaciens* as described above with minor modifications. The cell line 95.61.21 was used and after cefotaxime treatment for 2 days, cells were fixed and stained with DAPI. As a control, a pMDC32 vector containing the cDNA encoding for monomeric RFP (mRFP) was used.

Absolute quantitative RT-PCR analyses

q-RT-PCR was done as previously described (Moschou *et al.,* 2013). For absolute quantification of cDNA molecules in the RT-PCR, At *ESP* or Pa *ESP* in pGWB15 vectors were used as standards.

Preparation of Immunogen and Antibody

The pET11a-PaESP construct was transformed in BL21 (*DE3*) RIL (Stratagene) *Escherichia coli* cells. Purification of His-tagged recombinant C-terminal fragment containing C50 domain (1502-2307 aa) of Pa ESP was performed according to manufacturer instructions (Qiagen). Antisera were raised in three mice.

Western Blot Analysis

One hundred mg of plant material was mixed with 200 μL of 2x Laemmli sample buffer (Laemmli, 1970), kept on ice for 10 min and boiled for 5 min. Samples were centrifuged at 17,000*g* for 15 min. Equal amounts of each supernatant were loaded on 9% or 4-15% gradient polyacrylamide gels and blotted on PVDF (Polyvinylidene fluoride) membrane (see also Supplemental Methods). Anti-Pa ESP and anti-actin C4 were used at dilution 1:1,000 and 1:200, respectively; anti-mouse or anti-rat horseradish peroxidase (HRP)-conjugates (GE Healthcare, Sweden) were used at dilution 1:5,000. Blots were developed using ECL Prime kit (GE Healthcare, Sweden) and imaged in LAS-3000 Luminescent Image Analyzer (Fujifilm, Fuji Photo Film, Germany).

Immunocytochemistry and Imaging

Two-day-old early embryos of Norway spruce were fixed in 3.7% (w/v) formaldehyde in microtubule stabilizing buffer (MTSB; 0.1 M piperazine-N,N′-bis(2-ethanesulfonic acid) (PIPES), pH 6.8, 5 mM EGTA, 2 mM $MgCl_2$) supplemented with 1% (v/v) Triton X-100. Embryos were blocked with phosphate buffered saline Tween-20 (PBST) supplemented with 5% (w/v) bovine serum albumin (BSA; blocking solution). Subsequently, embryos were incubated overnight with anti-Pa ESP, diluted 1:500, and mouse anti-tubulin YL1/2 (AbD Serotec, UK), diluted 1:200 in blocking solution. Specimen were then washed three times for 30 min in PBST and incubated for 3 h with goat anti-mouse tetramethylrhodamine isothiocyanate (TRITC) and anti-rabbit fluorescein isothiocyanate (FITC) conjugated secondary antibodies diluted 1:200 in blocking solution. After washing in PBST, specimen were mounted in Vectashield (Vector Laboratories, Burlingame, CA) mounting medium. The samples were examined using a Leica SP5 or Zeiss 710 confocal microscopes. Objective lenses were oil-corrected 63x (NA=1.6) and samples were examined at room temperature.

Tissue Sectioning

Cotyledonary embryos were fixed for 2 h at room temperature under vacuum with 4% (w/v) paraformaldehyde in MTSB supplemented with 0.4% (v/v) Triton X-100. The fixative was washed away with PBST buffer, and embryos were dehydrated on ice by 0.85% (w/v) NaCl (30 min) and an EtOH gradient in 0.85% (w/v) NaCl (50, 70, 85, 95 and 100% for 90 min each, 100% overnight and 100% for 2 h). Samples were treated twice with 100% (v/v) xylene at room temperature for 1 h each, overnight with 50% (v/v) xylene supplemented with 50% (w/v) histowax at 40-50^{o}C, and 100% (w/v) histowax at 60^{o}C, changing twice per day for 3 consecutive days. Samples were stored at 4^{o}C until they were used. 10-µm thick sections were cut using a microtome and placed on poly-lysine coated slides in water droplets. Water was allowed to evaporate overnight at 45^{o}C. Samples were deparaffinised and rehydrated by two washes, 10 min each, in histoclear, two washes, 2 min each, in 100% (v/v) EtOH, followed by EtOH gradient (95, 90, 80, 60 and 30%) in PBS for 2 min each step. Slides were treated for 2 min with H_2O and 20 min with PBS. Sections were blocked and hybridized with antibodies as described above.

Microtubule and Image Analysis

Microtubule length was examined by measuring the length of individual end-to-end filaments in Z-stack images. Density of microtubules was calculated by projecting Z-stacks on single planes. The image and pixel analyses were done using ImageJ v1.48 software (rsb.info.nih.gov/ij). Default modules and options were used. Images were prepared using Adobe Photoshop CS6 (Adobe).

Statistical Analysis

Graphs were prepared using Excel v2013 (Microsoft) or JMP v11. Statistical analysis was performed with JMP v11. Statistical methods used are indicated in Figure legends.

Results

Identification, cloning and sequence analysis of Pa ESP

All known ESP proteins are encoded by single genes, with the only exception of *Drosophila melanogaster* ESP, which contains two subunits encoded by separate genes (reviewed in Moschou and Bozhkov, 2012). The full-length cDNA for Pa *ESP* was isolated by rapid amplification of cDNA ends (RACE), using internal primers that spanned the conserved 3'-end of the gene (File S1). The cDNA was sequenced and found to be 7,248-bp long and contained an open reading frame (ORF) encoding a polypeptide of 2,308 aa with predicted molecular mass of 259 kDa. We deposited Pa *ESP* sequence in GenBank under the accession number HE793991.1. Phylogenetic analysis revealed the monophyletic mode of ESP origin and that Pa ESP belongs to the gymnosperm clade located between mosses and angiosperms (Fig. 1a and File S1). The C-terminus of Pa ESP contains a conserved caspase-related proteolytic domain (Pfam number PF03568; aa 1673-2187, p=7.1e^{-88}; Fig. 1b) with the His, Cys catalytic dyad typical for all members of CD-clan proteases (Aravind and Koonin, 2002). This proteolytic domain is the most conserved region of Pa ESP exhibiting 30% and 31% identity with the corresponding domains of human and budding yeast homologues, and over 50% identity with plant homologues. The rest of the sequence is less conserved suggesting functional divergence within ESP family. In contrast to mammalian homologues, all plant ESP proteins lack a well-defined Leucine-rich region, which may be responsible for DNA binding (Fig. 1c; Sun *et al.*, 2009). Furthermore, Pa ESP lacks the Ca^{2+} binding EF-hand and 2Fe-2S motives identified in the *Arabidopsis* homologue (Fig. 1c). These differences in the primary sequence combined with monophyletic nature of the phylodendrogram suggest that ESP functions were fine-tuned in different lineages during evolution.

Pa ESP protein level is developmentally regulated

Early somatic embryos of Norway spruce develop from unorganized multicellular aggregates called proembryogenic masses (PEMs) upon withdrawal of plant growth regulators (PGR), auxin and cytokinin (Fig. 2a). The later stages of somatic embryogenesis resemble those of zygotic pathway and are promoted by abscisic acid (ABA; Filonova *et al.*, 2000). An early spruce embryo is composed of the embryonal mass, tube cells, and the suspensor (Fig. 2a). While the embryonal mass gives rise to the mature embryo, the suspensor is a transient structure undergoing programmed cell death (Filonova *et al.*, 2000). The tube cells are formed by

asymmetric division of stem-like cells in the embryonal mass. Each round of cell division produces two daughter cells with distinct fates; one retains proliferative capacity and remains within the embryonal mass, while its sister cell forms a transient type of cells known as tube cells. The tube cells elongate further to form suspensor cells (Bozhkov *et al.,* 2005).

To analyze the levels of Pa ESP at successive stages of plant development, we raised an antibody against the C50 catalytic domain of Pa ESP and used it in immunoblotting to detect Pa ESP in samples prepared at distinct stages of embryonic and post-embryonic development. The antibody recognized a protein of ca 260 kDa that corresponds to the predicted size of Pa ESP (Supporting Information, Methods). High levels of Pa ESP were detected in proliferating PEMs in the presence of PGR (+PGR), but not during differentiation of early embryos (-PGR; Fig. 2b), and in the microsurgically separated embryonal masses of early embryos (Fig. 2c). Neither suspensor cells nor distinct parts of seedlings including cotyledons, young needles, hypocotyls and roots contained detectable amount of Pa ESP protein, demonstrating that high levels of Pa ESP are associated with actively proliferating tissues. The level of Pa ESP seems to be regulated at the transcriptional level, since suspensor cells, cotyledons, hypocotyls and roots contained at least five times less Pa *ESP* mRNA levels than the embryonal mass (Fig. S1a).

Pa ESP localizes to microtubules and associates with the cell plate during cytokinesis

The intracellular localization of Pa ESP in the meristematic cells of PEMs and early embryos was examined using immunofluorescence microscopy (Fig. 3a). In non-dividing meristematic cells, Pa ESP decorated cortical microtubules (Fig. S2, top images), while during pre-prophase, Pa ESP was found on the pre-prophase band and perinuclear basket of microtubules (Fig. 3a, panel 1). At the beginning of prophase and until the onset of anaphase diffused localization of Pa ESP was detected around mitotic spindle, as well as on the kinetochore microtubules (Fig. 3a, panel 2). At the onset of anaphase, most of Pa ESP was associated with the spindle poles and midzone microtubules (Fig. 3a, panel 3 and Fig. 3b). This localization was independent of the fixation method since the same staining pattern was observed after more stringent fixation with methanol/acetone, which exposes epitopes masked by protein folding or interaction with other proteins (Fig. 3b). Densitometry profiling of the anaphase spindle revealed three apparent peaks corresponding to both spindle poles and the midzone (Fig. 3b). During telophase, Pa ESP concentrated in the phragmoplast midzone, where the cell plate is assembled (Fig. 3b, panel 4). A similar localization was observed after the

methanol/acetone fixation and the densitometry profiling revealed only one major peak of fluorescence in the phragmoplast midzone (Fig. 3c). Apart from the midzone, Pa ESP colocalized with microtubules at the leading edge of the phragmoplast, whilst missing in the midzone of the leading edge (Fig. 3a, inset in panel 4). At later stages of phragmoplast development, Pa ESP remained at the cell plate after the depolymerization of microtubules (Fig. 3a, panel 5).

We examined localization of Pa ESP in the first layer of anisotropically expanding cells adjacent to the embryonal mass, the tube cells. These cells cease proliferation becoming committed to programmed cell death. During the subsequent differentiation steps, the tube cells elongate to form stereotypical suspensor cells (Bozhkov et al. 2005; Smertenko and Bozhkov, 2014; Zhu *et al.*, 2014). Pa ESP was absent from these cells (Fig. S2, bottom images), consistent with the finding that Pa *ESP* mRNA level is greatly reduced in the suspensor (Fig. S1a).

Pa *ESP* deficiency impairs embryo development

To investigate the role of Pa *ESP* in embryogenesis we produced transgenic lines constitutively expressing a hairpin construct against Pa *ESP* (Pa *ESP*-RNAi; Fig. 4 and Fig. S1b). We could obtain only two viable cell lines (4.1 and 4.2), while the rest of transgenic lines ceased proliferation following initial selection. Both lines exhibited significantly lower levels of Pa ESP (Fig. 4a and Fig. S1b). Knockdown of Pa *ESP* inhibited the development of early embryos from PEMs upon withdrawal of PGR (Fig. 4b). Wild type (WT) cultures contained highly polarized embryos with compact embryonal masses and several files of anisotropically expanding suspensor cells. On the contrary, Pa *ESP*-RNAi lines contained irregularly formed embryonal masses connected to suspensor-like structure composed of cells with impaired anisotropic expansion (Fig. 4c and Fig. S3a). These cells were excluded from the embyonal masses implying that Pa ESP does not affect specification of tube or suspensor cells, but they failed to elongate and formed large suspensor-like structure with significantly more cells in a file, when compared to WT embryos (Fig. S3a). We noticed that some distal cells of the embryo in RNAi lines exhibited apparent signs of cell death (staining with Evan's blue; Fig. S4). However, these cells lacked signs of proper anisotropic expansion.

To exclude the possibility that observed phenotype was a consequence of the pleiotropic effects of the constitutive depletion of Pa *ESP*, we generated estradiol inducible Pa *ESP* RNAi lines (Pa *ESP*-XVE>RNAi; Fig. S1a). Depletion of Pa ESP after treatment with estradiol

(induction was done from early embryogenesis onwards) induced similar developmental defects as described for constitutive RNAi lines (Fig. S3a, b). Yet, no alteration in embryo morphology was observed in the Pa *ESP*-XVE>RNAi lines in the absence of estradiol. Taken together, these data demonstrate that Pa ESP is essential for anisotropic cell expansion following the first asymmetric cell division during embryogenesis.

Pa ESP is required for chromosome disjunction

To investigate the role of Pa ESP in execution of sister chromatid separation, we stained Pa *ESP*-RNAi or Pa *ESP*-XVE>RNAi cells with DAPI (Fig. 5). We failed to identify any discernible chromosomal aberrations suggesting that during selection process we most likely counter-selected for lines that have sufficient levels Pa ESP to sustain cell division. Furthermore, stable transformation with Pa *ESP*-XVE>RNAi also failed suppressing Pa *ESP* below 50% of the original level in 12 lines despite various induction regimes (estradiol concentration ranging from 1 μM to 50 μM during early embryogenesis).

We overcome this limitation by the transient expression of the Pa *ESP*-RNAi construct mediated by *Agrobacterium tumefaciens* (see Material and Methods for the establishment of the protocol). We used a control vector expressing monomeric RFP (mRFP) to estimate the percentage of cells transformed following *A. tumefaciens* transfection. Approximately, 80% showed detectable mRFP expression under confocal microscope. Transient depletion of Pa *ESP* resulted in over 90% reduction of Pa *ESP* levels, when compared to mRFP transfected cells (determined by qRT-PCR; see also Materials and Methods). We assume that some cells should have even higher suppression of Pa *ESP*, considering that ca. 20% of cells may not be transfected with the RNAi construct. Analysis of the transfected cells revealed chromosome non-disjunction phenotype (Fig. 5; 12 of 56 cells examined versus none of 67 in mRFP control) resembling *Arabidopsis rsw4* allele in this context (Moschou *et al.*, 2013). Complementation experiments of *Arabidopsis rsw4* phenotype with Pa *ESP* showed that Pa ESP could rescue chromatid non-disjunction phenotype of *rsw4* (Liu and Makaroff, 2006; Fig. S5d), but failed to rescue the root swelling phenotype (Fig. S5a-c). On the other hand, a point mutant of Pa ESP with a catalytic cysteine-to-glycine mutation failed to rescue chromatid non-disjuction (data not shown). Thus, Pa ESP performs the canonical role of ESP proteins in anaphase progression.

Pa ESP is essential for the late embryogenesis

We next compared the later stages of embryogenesis in WT and Pa ESP-deficient lines (Fig. 6 and Fig. S6). Whereas normally the cotyledonary embryos could be detected following two weeks after transfer to the maturation medium containing ABA, the cotyledonary embryos in Pa *ESP*-RNAi or Pa *ESP*-XVE>RNAi lines formed only after 10 weeks (Fig. 6a and Fig. S6a, b). The cotyledonary embryos that eventually formed in the RNAi lines exhibited a range of morphological abnormalities, including misshaped and missing cotyledons, short hypocotyls, and split embryos (Fig. 6b, c). Histological examination revealed that individual cortical cells in the hypocotyls of the cotyledonary embryos were enlarged, while the meristematic regions were markedly reduced (Fig. 6d, e and Fig. S6c). Microscopic examination of the DNA staining with DAPI revealed the lack of chromosome non-disjunction phenotype in these lines, suggesting that these developmental defects are not caused by chromosomal aberrations. Therefore, the role of ESP in regulating cell expansion seems to be mechanistically unrelated to its role in anaphase progression.

Pa ESP deficiency affects microtubule stability

Since polarized development depends on cell expansion controlled by microtubules, we examined their organization in the elongating suspensor cells. The highly fragmented nature of microtubules in elongating suspensor cells (see also Smertenko *et al.,* 2003) prevented us from drawing conclusions on microtubule architecture in these cells. We analyzed microtubule organization in two cell types of early embryos: (i) the meristematic cells of the embryonal mass and (ii) embryonal tube cells. Knockdown of Pa *ESP* caused no significant alterations in the random organization of cortical microtubules in the embryonal mass cells (Fig. 7a; Smertenko et al. 2003). Contrary, cortical microtubules in the tube cells of Pa *ESP*-RNAi showed reduced density and length (Fig. 7a-c). Similarly, the density and length of cortical microtubules in the hypocotyl cells of Pa *ESP*-RNAi cotyledonary embryos were reduced (Fig. 7a-c). Furthermore, while majority (ca 70%) of microtubules in the hypocotyl cells of cotyledonary WT embryos were transverse, they became predominantly oblique or longitudinal in the Pa *ESP*-RNAi lines (Fig. 7d, e). Taken together, these results demonstrate that despite significant reduction of Pa ESP expression during cell differentiation, its activity remains critical for the regulation of microtubule organization and for cell elongation.

Discussion

Diversification of ESP proteins

All members of ESP family share caspase-hemoglobinase fold characteristic for CD clan of cysteine proteases, which includes clostripains, legumains, gingipains, caspases, paracaspases and metacaspases (Aravind and Koonin, 2002). Apart of this conserved fold, the primary structure of ESP lacks significant conservation (Fig. S1). For example, Pa ESP is devoid of the Ca^{2+}-binding EF-hand and 2Fe-2S motives found in At ESP. However, whether these motives serve any function remains unclear.

Phylogenetic analysis reveals that ESP homologues of green, brown and diatom algae, and land plants form independent clades (Fig. 1a). This pattern suggests that besides the role in daughter chromatid disjunction, ESP evolved specific functions in each lineage. The monophyletic nature of land plant clade indicates that structure and functions of ESP co-evolved with increased complexity of morphology and life cycle. Considering paucity of information on ESP in *Charophytes*, it remains inconclusive whether primary structure of ESP in land plants diverged due to the evolution of phragmoplast, colonization of land, or transition from unicellular to multicellular body plan (Leliaert *et al.,* 2011). The latter reason can however be ruled out because ESP homologues from unicellular green algae form two separate clades and ESP from multicellular brown algae *Ectocarpus siliculosus* does not group together with any other proteins (Fig. 1a).

Role of Pa ESP in cell division and microtubule organization

ESP from different lineages reveal variable intracellular localization pattern. Yeast ESP associates with spindle poles and microtubules of anaphase spindle, whereas human ESP was found only on the metaphase spindle poles and then became cytoplasmic in anaphase (Jensen *et al.,* 2001; Chestukhin *et al.,* 2003). *Arabidopsis* ESP associates with microtubules of prophase, metaphase and anaphase spindle, as well as phragmoplast microtubules and cell plate (Moschou *et al.,* 2013).

Similar to At ESP, Pa ESP associates with microtubules during interphase, prophase, metaphase and anaphase and then associates with the phragmoplast microtubules, midzone and cell plate during telophase. Interestingly, Pa ESP was missing from the midzone of the phragmoplast leading edge. Therefore, Pa ESP appears to lack binding sites during initiation of the cell plate assembly. Pa ESP remains associated with the cell plate after disassembly of

phragmoplast microtubules, suggesting that it might be required for vesicle trafficking to the maturing cell plate. Consistent with this conclusion, At ESP was found to be temporally colocalized with RabA2a-specific endosomes (Moschou *et al.,* 2013).

In our experiments constitutive down-regulation of Pa ESP did not result in chromosome non-disjunction and cytokinetic defects observed in other systems, including *Arabidopsis* (Fig. 5; Liu and Makaroff, 2006; Wu *et al.,* 2010; Moschou *et al.,* 2013). Furthermore, despite association of Pa ESP with mitotic microtubule arrays, no discernible abnormalities in their organization were observed in the Pa *ESP*-RNAi lines. The most likely explanation of normal cell divisions in the Pa *ESP*-RNAi lines is the incomplete gene silencing still allowing production of a sufficient amount of protein (Fig. 4a, upper panel) that sustains anaphase transition. Accordingly, more efficient reduction of Pa ESP by using the transient transfection method that we established herein, revealed the requirement of Pa ESP for chromosome disjunction. Therefore, Pa ESP plays a canonical role in anaphase progression. Although in constitutive RNAi lines the level of Pa ESP was sufficient to ensure normal anaphase progression, the reduced number of meristematic cells in the hypocotyls of Pa ESP-deficient embryos suggests that Pa ESP is required for the regulation of meristem size, independently of its role in anaphase.

Consistent with the specific functions of ESP in different lineages, Pa ESP failed to rescue the root-swelling phenotype of *Arabidopsis rsw4* although previously this phenotype could be complemented by At ESP (Moschou *et al.,* 2013). Considering that Pa ESP could complement the chromosome non-disjunction phenotype of *rsw4* and its knock down results in the non-disjunction, Pa ESP appears to be a functional homologue of canonical ESP proteins. These findings suggest different molecular mechanisms underlying the functions of ESP in anaphase progression and in controlling anisotropic cell expansion.

In contrast to the unaltered microtubule arrays in the embryonal masses, the cortical microtubules in tube cells and especially in epidermis and cortex cells of cotyledonary embryos of Pa *ESP*-RNAi lines exhibited reduced density and length, as well as altered orientation. The hypocotyl cells in the Pa ESP-deficient embryos were bigger than in the WT, indicating that abnormal microtubule organization was associated with irregular cell expansion (Baskin, 2001; Wasteneys, 2004; Baskin and Gu, 2012). This implies that regulation of microtubule dynamics in cells engaged in anisotropic growth are more sensitive to loss of Pa ESP function than proliferating cells of early embryos, which can tolerate the reduced accumulation of Pa ESP. Therefore, Pa ESP

could facilitate stabilization of microtubules which define the elongation axis. We assume that Pa ESP function in stabilization of microtubules could be non-cell-autonomous, involving mobile signals produced in meristematic cells. This function of Pa ESP is consistent with our findings that elongating cells with undetectable Pa ESP (e.g. tube cells) are affected when Pa ESP is depleted in proximal meristematic cells (e.g. embryonal mass cells).

Pa ESP is required for elongation of the suspensor

Spruce embryo at the early embryogeny stage undergoes polarization and forms two domains with distinct developmental fates: proliferating embryonal mass and terminally-differentiated suspensor, including the uppermost layer of tube cells (Fig. 2a; Bozhkov *et al.*, 2005). Pa ESP protein could be detected using antibody only in the embryonal masses, while the level of protein accumulation in the elongating embryo-suspensors, tube cells, and seedlings was below detection limits. In accordance with the Western blotting data, qRT-PCR demonstrated significant down-regulation of ESP in all organs, but embryonal mass.

Our reverse genetics experiments demonstrate that Pa ESP is critically required to sustain cell elongation during embryogeny. Developmental defects induced by Pa ESP deficiency resemble the phenotype of spruce embryos grown in the presence of polar auxin transport inhibitor, 1-N-naphtylphthalamic acid (Larsson *et al.*, 2008). For example, in both cases the fate of suspensor cells was affected and supernumerary suspensor-like cells could be detected instead of normally elongating cells. It is tempting to speculate that as in *Arabidopsis* root cells (Moschou *et al.*, 2013), inhibition of Pa ESP perturbs auxin signaling and in this way interferes with cell expansion.

Conclusion

Here, we were able to dissect two functions of separase by showing that a gymnosperm homologue could complement chromosome non-disjunction phenotype of *rsw4*, but not the root swelling phenotype. This cell division-unrelated function of separase could be attributed to the regulation of polarized vesicular trafficking. So far no robust molecular markers of cell polarity have been established for gymnosperms, however recent advances in gymnosperm genomics and an increasing number of fully sequenced gymnosperm genomes should help to overcome these limitations (Birol *et al.*, 2013; Nystedt *et al.*, 2013; Zimin *et al.*, 2014).

Acknowledgments

Authors are grateful to Tsuyoshi Nakagawa for sharing published research materials and Alison Ritchie for the assistance in preparation of anti-Pa ESP. This work was supported by grants from the VR Swedish Research Council (to P.N.M. and P.V.B.), Pehrssons Fund (to P.V.B.), the Swedish Foundation for Strategic Research (to P.V.B.), Olle Engkvist Foundation (to P.V.B.), Knut and Alice Wallenberg Foundation (to P.V.B.), August T. Larsson Foundation (to A.P.S. and P.V.B.), Hatch Grant WNP00826 (to A.P.S.), and a Spanish Ministry of Science and Innovation grant (AGL2010-15684 to M.F.S). V. S-V was recipient of a FPI fellowship from the Spanish Ministry of Science and Innovation (BES-2008-003592).

Author contributions

P.N.M., E.I.S., E.A.M., K.F.M. S.H.R., E.G.-B. and V.S.-V., performed research; P.N.M., A.P.S., P.V.B., designed research; P.N.M., A.P.S., P.V.B. wrote this article; M.F.S. and P.J.H. offered materials/analytical methods. All authors approved the final version of the manuscript.

References

Aravind L, Koonin EV. 2002. Classification of the caspase-hemoglobinase fold: detection of new families and implications for the origin of the eukaryotic separins. Proteins **46:** 355-367.

Baskin TI. 2001. On the alignment of cellulose microfibrils by cortical microtubules: a review and a model. *Protoplasma* **215:** 150-171.

Baskin TI, Gu Y. 2012. Making parallel lines meet: transferring information from microtubules to extracellular matrix. *Cell Adhesion and Migration* **6:** 404-408.

Bembenek JN, White JG, Zheng YX. 2010. A role for separase in the regulation of RAB-11-positive vesicles at the cleavage furrow and midbody. *Current Biology* **20:** 259-264.

Birol I, Raymond A, Jackman SD, Pleasance S, Coope R, Taylor GA, Saint Yuen MM, Keeling CI, Brand D, Vandervalk BP, et al. 2013. Assembling the 20 Gb white spruce (*Picea glauca*) genome from whole-genome shotgun sequencing data. *Bioinformatics* **29:** 1492-1497.

Bozhkov PV, Filonova LH, Suarez MF. **2005.** Programmed cell death in plant embryogenesis. *Current Topics in Developmental Biology* **67:** 135-179.

Brand L, Horler M, Nuesch E, Vassalli S, Barrell P, Yang W, Jefferson RA, Grossniklaus U, Curtis MD. 2006. A versatile and reliable two-component system for tissue-specific gene induction in *Arabidopsis*. *Plant Physiology* **141:** 1194–1204.

Capron A, Chatfield S, Provart N, Berleth T. 2009. Embryogenesis: pattern formation from a single cell. *Arabidopsis Book* **7:** e0126.

Chestukhin A, Pfeffer C, Milligan S, DeCaprio JA, Pellman D. 2003. Processing, localization, and requirement of human separase for normal anaphase progression. *Proceedings of the National Academy of Sciences of the United States of America* **100:** 4574-4579.

Ciosk R, Zachariae W, Michaelis C, Shevchenko A, Mann M, Nasmyth K. 1998. An ESP1/PDS1 complex regulates loss of sister chromatid cohesion at the metaphase to anaphase transition in yeast. *Cell* **93:** 1067-1076.

Filonova LH, Bozhkov PV, Brukhin VB, Daniel G, Zhivotovsky B, von Arnold S. 2000. Two waves of programmed cell death occur during formation and development of somatic embryos in the gymnosperm, Norway spruce. *Journal of Cell Science* **24:** 4399-4411.

Filonova LH, Suarez MF, Bozhkov PV. 2008. Detection of programmed cell death in plant embryos. *Methods in Molecular Biology* **427:** 173-179.

Jensen S, Segal M, Clarke DJ, Reed SI. 2001. A novel role of the budding yeast separin Esp1 in anaphase spindle elongation: evidence that proper spindle association of Esp1 is regulated by Pds1. *Journal of Cell Biology* **152:** 27-40.

Johnson KL, Degnan KA, Walker JR, Ingram GC. 2005. AtDEK1 is essential for specification of embryonic epidermal cell fate. *Plant Journal* **44:** 114-127.

Kanei M, Horiguchi G, Tsukaya H. 2012. Stable establishment of cotyledon identity during embryogenesis in Arabidopsis by ANGUSTIFOLIA3 and HANABA TARANU. *Development* **139:** 2436-2446.

Laemmli UK. 1970. Cleavage of structural proteins during the assembly of the head of bacteriophage T4. *Nature* **227:** 680-685.

Larsson E, Sitbon F, Ljung K, von Arnold S. 2008. Inhibited polar auxin transport results in aberrant embryo development in Norway spruce. *New Phytologist* **177:** 356-366.

Leliaert F, Verbruggen H, Zechman FW. 2011. Into the deep: New discoveries at the base of the green plant phylogeny. *Bioessays* **33:** 683-692.

Lid SE, Olsen L, Nestestog R, Aukerman M, Brown RC, Lemmon B, Mucha M, Opsahl-Sorteberg HG, Olsen OA. 2005. Mutation in the *Arabidopisis thaliana* DEK1 calpain gene perturbs endosperm and embryo development while over-expression affects organ development globally. *Planta* **221:** 339-351.

Liu Z, Makaroff CA. 2006. *Arabidopsis* separase *AESP* is essential for embryo development and the release of cohesin during meiosis. *Plant Cell* **18:** 1213-1225.

Mayer U, Ruiz RAT, Berleth T, Misera S, Jurgens G. 1991. Mutations Affecting Body Organization in the *Arabidopsis* Embryo. *Nature* **353:** 402-407.

Meinke DW. 1991. Perspectives on genetic-analysis of plant embryogenesis. *Plant Cell* **3:** 857-866.

Minina EA, Filonova LH, Fukada K, Savenkov EI, Gogvadze V, Clapham D, Sanchez-Vera V, Suarez MF, Zhivotovsky B, et al. 2013. Autophagy and metacaspase determine the mode of cell death in plants. *Journal of Cell Biology* **203:** 917-927.

Moschou PN, Bozhkov PV. 2012. Separases: biochemistry and function. *Physiologia Plantarum* **145:** 67-76.

Moschou PN, Smertenko AP, Minina EA, Fukada K, Savenkov EI, Robert S, Hussey PJ, Bozhkov PV. 2013. The caspase-related protease separase (*EXTRA SPINDLE POLES*) regulates cell polarity and cytokinesis in Arabidopsis. *Plant Cell* **25:** 2171-2186.

Nakagawa T, Kurose T, Hino T, Tanaka K, Kawamukai M, Niwa Y, Toyooka K, Matsuoka K, Jinbo T, Kimura T. 2007. Development of series of gateway binary vectors, pGWBs, for realizing efficient construction of fusion genes for plant transformation. *Journal of Biosciences and Bioengineering* **104:** 34-41.

Nystedt B, Street NR, Wetterbom A, Zuccolo A, Lin YC, Scofield DG, Vezzi F, Delhomme N, Giacomello S, Alexeyenko A, et al. 2013. The Norway spruce genome sequence and conifer genome evolution. *Nature* **497:** 579-584.

Pennell RI, Janniche L, Scofield GN, Booij H, Devries SC, Roberts K. 1992. Identification of a transitional cell state in the developmental pathway to carrot somatic embryogenesis. *Journal of Cell Biology* 119: 1371-1380.

Saitou N, Nei M. 1987. The Neighbor-Joining method-a new method for reconstructing phylogenetic trees. *Molecular Biology and Evolution* **4:** 406-425.

564 **Singh HE. 1978.** Embryology of gymnosperms. In: Handbuch der Pflanzenanatomie, Berlin,
565 Germany: Gebruder Borntraeger.
566 **Smertenko A, Bozhkov PV. 2014.** Somatic embryogenesis: life and death processes during
567 apical-basal patterning. *Journal of Experimental Botany* **65:** 1343-1360.
568 **Smertenko AP, Bozhkov PV, Filonova LH, von Arnold S, Hussey PJ. 2013.** Re-organisation
569 of the cytoskeleton during developmental programmed cell death in Picea abies embryos. *Plant*
570 *Journal* **33:** 813-824.
571 **Suarez MF, Filonova LH, Smertenko A, Savenkov EI, Clapham DH, von Arnold S,**
572 **Zhivotovsky B, Bozhkov PV. 2004.** Metacaspase-dependent programmed cell death is essential
573 for plant embryogenesis. *Current Biology* **14:** R339-R340
574 **Sun YX, Kucej M, Fan HY, Yu H, Sun QY, Zou H. 2009.** Separase is recruited to mitotic
575 chromosomes to dissolve sister chromatid cohesion in a DNA-dependent manner. *Cell* **137:** 123-
576 132.
577 **Tanaka H, Onouchi H, Kondo M, Hara-Nishimura I, Nishimura M, Machida C, Machida Y.**
578 **2001.** A subtilisin-like serine protease is required for epidermal surface formation in *Arabidopsis*
579 embryos and juvenile plants. *Development* **128:** 4681-4689.
580 **Ueda M, Laux T. 2012.** The origin of the plant body axis. *Current Opinion in Plant Biology* **15:**
581 578-584.
582 **van der Hoorn RAL. 2008.** Plant proteases: From phenotypes to molecular mechanisms. *Annual*
583 *Review of Plant Biology* **59:** 191-223.
584 **von Arnold S, Sabala I, Bozhkov P, Dyachok J, Filonova L. 2002.** Developmental pathways of
585 somatic embryogenesis. *Plant Cell Tissue and Organ Culture* **69:** 233-249.
586 **Wasteneys GO. 2004.** Progress in understanding the role of microtubules in plant cells. *Current*
587 *Opinion in Plant Biology* **7:** 651-660
588 **Wendrich JR, Weijers D. 2013.** The Arabidopsis embryo as a miniature morphogenesis model.
589 *New Phytologist* **199:** 14-25.
590 **Wu S, Scheible WR, Schindelasch D, Van Den Daele H, De Veylder L, Baskin TI. 2010.** A
591 conditional mutation in *Arabidopsis thaliana* separase induces chromosome non-disjunction,
592 aberrant morphogenesis and cyclin B1;1 stability. *Development* **137:** 953-961.

Yang XH, Boateng KA, Yuan L, Wu S, Baskin TI, Makaroff CA. 2011. The *Radially Swollen 4* separase mutation of *Arabidopsis thaliana* blocks chromosome disjunction and disrupts the radial microtubule system in meiocytes. *Plos One* 6

Zhu T, Moschou PN, Alvarez JM, Sohlberg JJ, von Arnold S. 2014. Wuschel-related homeobox 8/9 is important for proper embryo patterning in the gymnosperm Norway spruce. *Journal of Experimental Botany* **65:** 6543-6552.

Zimin A, Stevens KA, Crepeau M, Holtz-Morris A, Koriabine M, Marcais G, Puiu D, Roberts M, Wegrzyn JL, de Jong PJ, Neale DB, et al. 2014. Sequencing and assembly of the 22-Gb loblolly pine genome. *Genetics* **196:** 875-890.

Figure legends

Figure 1. Analysis of Pa ESP sequence.

(a) Phylodendrogram of ESP protein homologues. *Saccharomyces cerevisiae* protein sequence was used as an out-group. The bootstrap value for all branching points is 100% unless indicated otherwise. Accession numbers are indicated in Supplemental File 1.

(b) Alignment of aa sequences corresponding to the C50 proteolytic domain of ESP proteins. At, *Arabidopsis thaliana*; Rc, *Ricinus communis*; Dm, *Drosophila melanogaster*; Sc, *Saccharomyces cerevisiae*; Ce, *Caenorhabditis elegans*; Sp; *Schizosaccharomyces pombe*; Hs, *Homo sapiens*; Cr, *Cryptosporidium parvum*; Cm, *Chlamydomonas reinhardtii*; Pa, *Picea abies*. Asterisks denote the conserved His, Cys dyad.

(c) Domain organization of selected members of ESP family proteases. C50, proteolytic domain; LR, Leu-rich domain; EF-hand, helix-loop-helix topology with the ability to bind Ca^{2+}; 2Fe-2S, iron-sulfur cluster.

Figure 2. Pa ESP level is developmentally regulated.

(a) A schematic model (adapted from Filonova *et al.,* 2000) and corresponding micrographs of three principal stages of spruce somatic embryogenesis. Red and blue colors denote proliferating and dying cells, respectively. EM, embryonal mass; PGR, plant growth regulators; ABA, abscisic acid. Scale bars, 100 μm.

(b) Western blot analysis of Pa ESP in 2-day-old embryogenic culture grown in the presence (+PGR) or absence (-PGR) of PGR.

(c) Western blot analysis of Pa ESP in the embryonal masses (EM) and suspensors (SUS) of early somatic embryos, as well as in cotyledons (C), young needles (YN), hypocotyls (H) and roots (R) of seedlings. The images of plant material used for protein extraction are shown above the western blot.

Figure 3. Intracellular localization of Pa ESP.

(a) Staining of Pa ESP, tubulin, and DNA in the embryonic cells fixed with formaldehyde during prophase (1), metaphase (2), anaphase (3), telophase (4) and late cytokinesis (5). Inset in panel 4 shows higher magnification of the phragmoplast leading edge. Arrowhead denotes the absence of Pa ESP in the leading edge. Inset in panel 5 shows maximum projection image with DNA staining. Scale bars, 5 μm.

(b) and **(c)** Staining of Pa ESP, tubulin and DNA in the embryonic cells fixed with methanol during anaphase (B) and telophase (C). Densitometry scans were performed in the framed areas. Scale bars, 5 μm.

Figure 4. Effect of Pa *ESP* knockdown on early embryogenesis.

(a) Western blot analysis of Pa ESP in wild type (WT) and Pa *ESP*-RNAi cell lines. The equal loading was confirmed using anti-actin.

(b) Ratio of early embryos to PEMs in WT and Pa *ESP*-RNAi lines grown for seven days without PGR. The data show mean ± standard deviation of triplicate experiments. *, $P<0.01$; *vs* WT, Student's *t*-test.

(c) Representative dark field microscopy images of early embryos from WT and Pa *ESP*-RNAi lines grown for seven days without PGR. Arrows indicate formation of ectopic files of small cells instead of elongated suspensor cells. EM, embryonal mass. Scale bars, 100 μm.

Figure 5. Chromosomal aberrations in cells with transiently diminished Pa *ESP*

For detection of chromosomal aberrations cells were fixed and stained with DAPI. Images are from a single representative experiment replicated twice. As a control in transient assays, lines transiently expressing mRFP under a 35S promoter were used. Aberrations were never observed in these transformants. Arrowhead indicates chromosomal aberration. Yellow lines indicate cell wall between chromosomes of daughter cells. trans, transient. Scale bars, 5 μm.

Figure 6. Effect of Pa *ESP* knockdown on development of cotyledonary embryos.

(a) Time course analysis of cotyledonary embryo formation in WT and Pa *ESP*-RNAi line 4.1. Data are from a single representative experiment, which was repeated twice with similar results.

(b) Classes of cotyledonary embryo phenotypes observed in WT and Pa *ESP*-RNAi line 4.1. Normal, cotelydonary embryos showing radial symmetry and average size; weak, cotelydonary embryos with disturbed radial symmetry and decreased size; severe, cotelydonary embryos showing scission and/or loss of radial symmetry and/or size aberrations; mild, in between the weak and severe classes. Scale bars, 5 mm.

(c) Frequency distribution of distinct phenotypes of cotyledonary embryos in WT and Pa *ESP*-RNAi line 4.1. Note the absence of normal embryos in the RNAi line. Data are from a single representative experiment, which was repeated twice.

(d) Longitudinal sections of hypocotyls of cotyledonary embryos from WT and Pa *ESP*-RNAi line 4.1. Shown on the right are enlarged boxed areas. Yellow lines demarcate meristematic regions. Scale bar, 300 μm.

(e) Diameter of hypocotyl cortex cells of cotyledonary embryos from WT and Pa *ESP*-RNAi lines. The data show mean ± standard deviation of triplicate experiments, each containing at least 10 tissue sections. *, $P<0.01$; *vs* WT, Student's *t*-test.

Figure 7. Effect of Pa *ESP* knockdown on the organization of cortical microtubules.

(a) Organization of cortical microtubules in embryonal mass and tube cells of early embryos and hypocotyl cells of cotyledonary embryos from WT and Pa *ESP*-RNAi line 4.1. Insets show higher magnification of boxed areas. Scale bars, 10 μm.

(b) and **(c)** Microtubule length and density (number of microtubules per 10 μm) in the embryonal tube cells and hypocotyl cells from WT and Pa *ESP*-RNAi line 4.1. The data show mean ± standard deviation of duplicate experiments, each including 27 (**b**) or 10 (**c**) cells analyzed. *, $P<0.05$; *vs* WT, two-sided Dunnett's test.

(d) Orientation of microtubules (percentage of microtubules in each particular orientation) in the hypocotyl cells from WT and Pa *ESP*-RNAi line 4.1. Data are from a single representative experiment, which was repeated twice, each time including 27 cells analyzed. *, $P<0.05$; vs WT, Fischer's exact test.

685 **(e)** Schematic model for the organization of microtubules in the hypocotyls of WT and Pa *ESP*-
686 RNAi embryos. In the WT embryos, microtubules have predominantly transverse orientation and
687 cells expand anisotropically. In the Pa *ESP*-RNAi embryos, microtubules are disorientated, shorter
688 and less dense and cells expand isotropically.
689

690 **Supporting Information**

691 Additional supporting information may be found in the online version of this article.

692 **Fig. S1. Relative expression levels of Pa *ESP* in WT, Pa *ESP*-RNAi or Pa *ESP*XVE> RNAi**
693 **lines.**

694 **Fig. S2. Intracellular localization of Pa ESP in interphase embryonal mass cells and**
695 **differentiated tube cells.**

696 **Fig. S3. Width, length and number of tube and suspensor cells and potency for embryo**
697 **formation, as affected by Pa ESP deficiency.**

698 **Fig. S4. Evan's blue staining of suspensor cells in WT and Pa ESP-RNAi.**
699

700 **Fig. S5. Pa *ESP* does not complement *rsw4* root swelling phenotype but complements the**
701 **chromatid non-disjunction phenotype.**
702

703 **Fig. S6. Effect of inducible Pa *ESP* knockdown on the morphology of cotyledonary embryos.**
704

705 **Table S1. List of primers.**

706 **Methods S1. Western blot analysis of Pa ESP protein.**

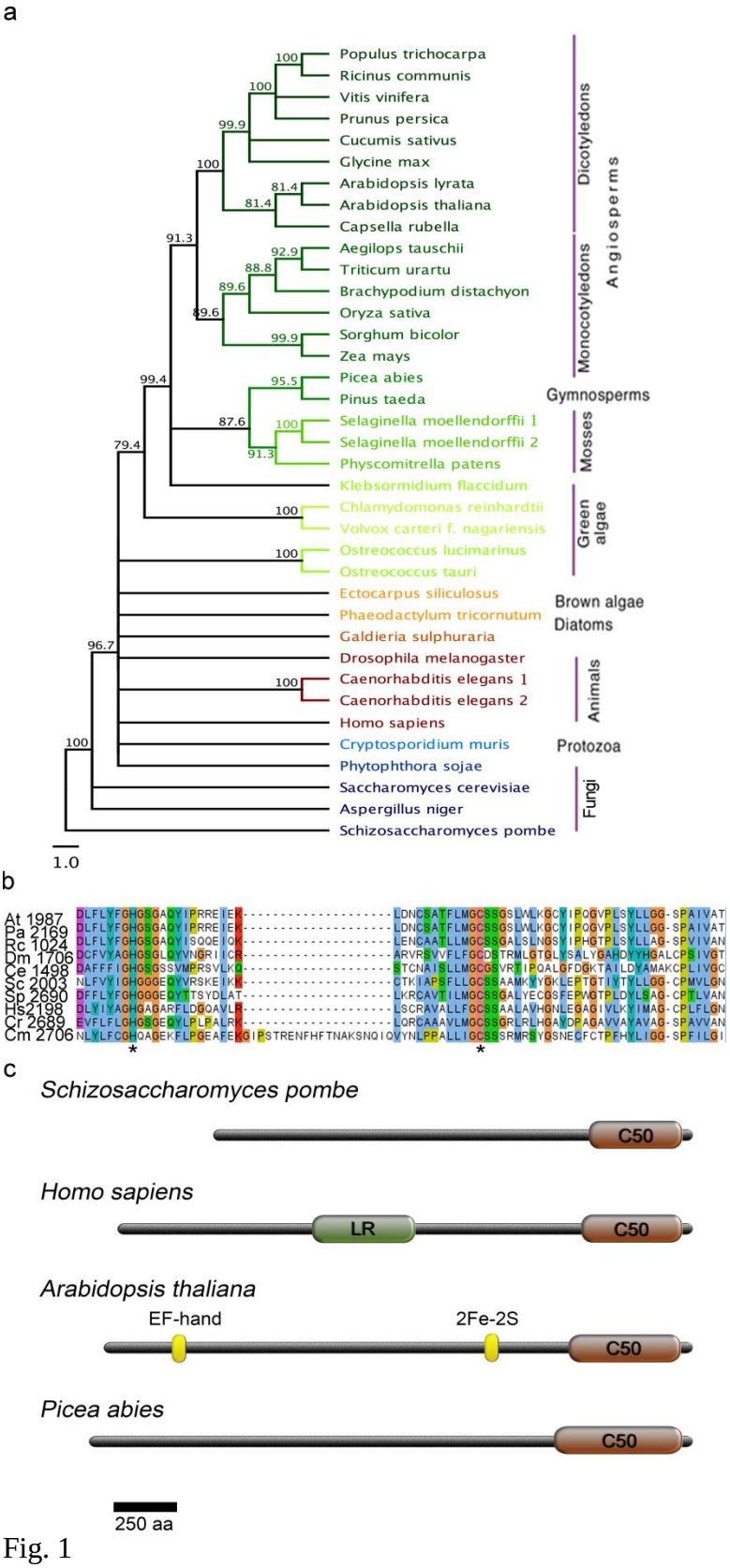
a
Populus trichocarpa
Ricinus communis
Vitis vinifera
Prunus persica
Cucumis sativus
Glycine max
Arabidopsis lyrata
Arabidopsis thaliana
Capsella rubella
Aegilops tauschii
Triticum urartu
Brachypodium distachyon
Oryza sativa
Sorghum bicolor
Zea mays
Picea abies
Pinus taeda
Selaginella moellendorffii 1
Selaginella moellendorffii 2
Physcomitrella patens
Klebsormidium flaccidum
Chlamydomonas reinhardtii
Volvox carteri f. nagariensis
Ostreococcus lucimarinus
Ostreococcus tauri
Ectocarpus siliculosus
Phaeodactylum tricornutum
Galdieria sulphuraria
Drosophila melanogaster
Caenorhabditis elegans 1
Caenorhabditis elegans 2
Homo sapiens
Cryptosporidium muris
Phytophthora sojae
Saccharomyces cerevisiae
Aspergillus niger
Schizosaccharomyces pombe
1.0
Dicotyledons
Monocotyledons
Angiosperms
Gymnosperms
Mosses
Green algae
Brown algae
Diatoms
Animals
Protozoa
Fungi
b
At 1987
Pa 2169
Rc 1024
Dm 1706
Ce 1498
Sc 2003
Sp 2690
Hs2198
Cr 2689
Cm 2706
c
Schizosaccharomyces pombe
C50
Homo sapiens
LR
C50
Arabidopsis thaliana
EF-hand
2Fe-2S
C50
Picea abies
C50
250 aa

Fig. 1

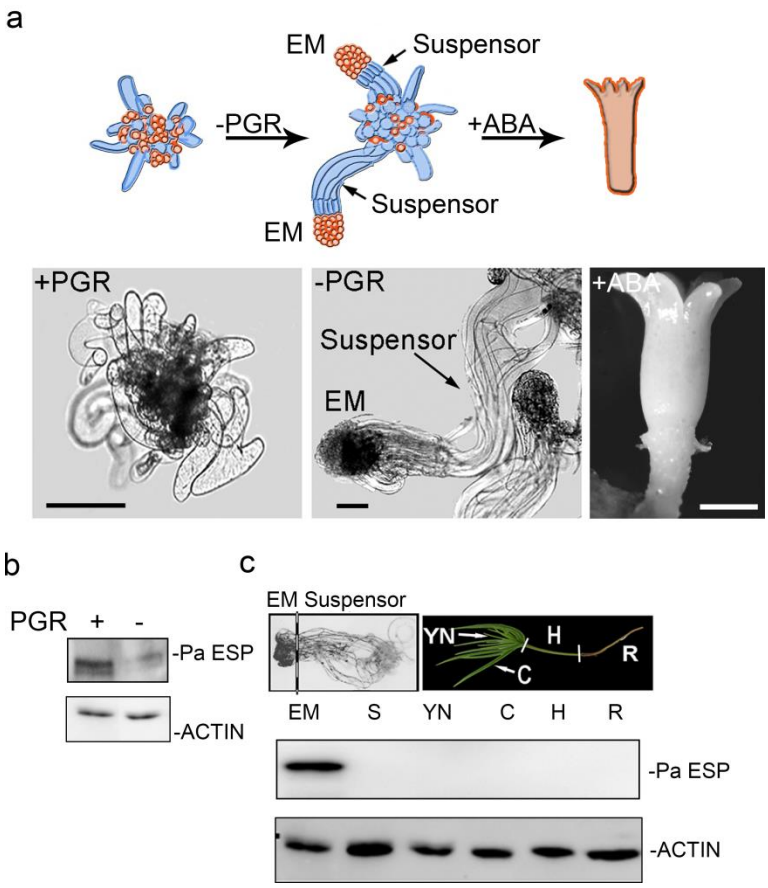

709
710 Fig. 2
711

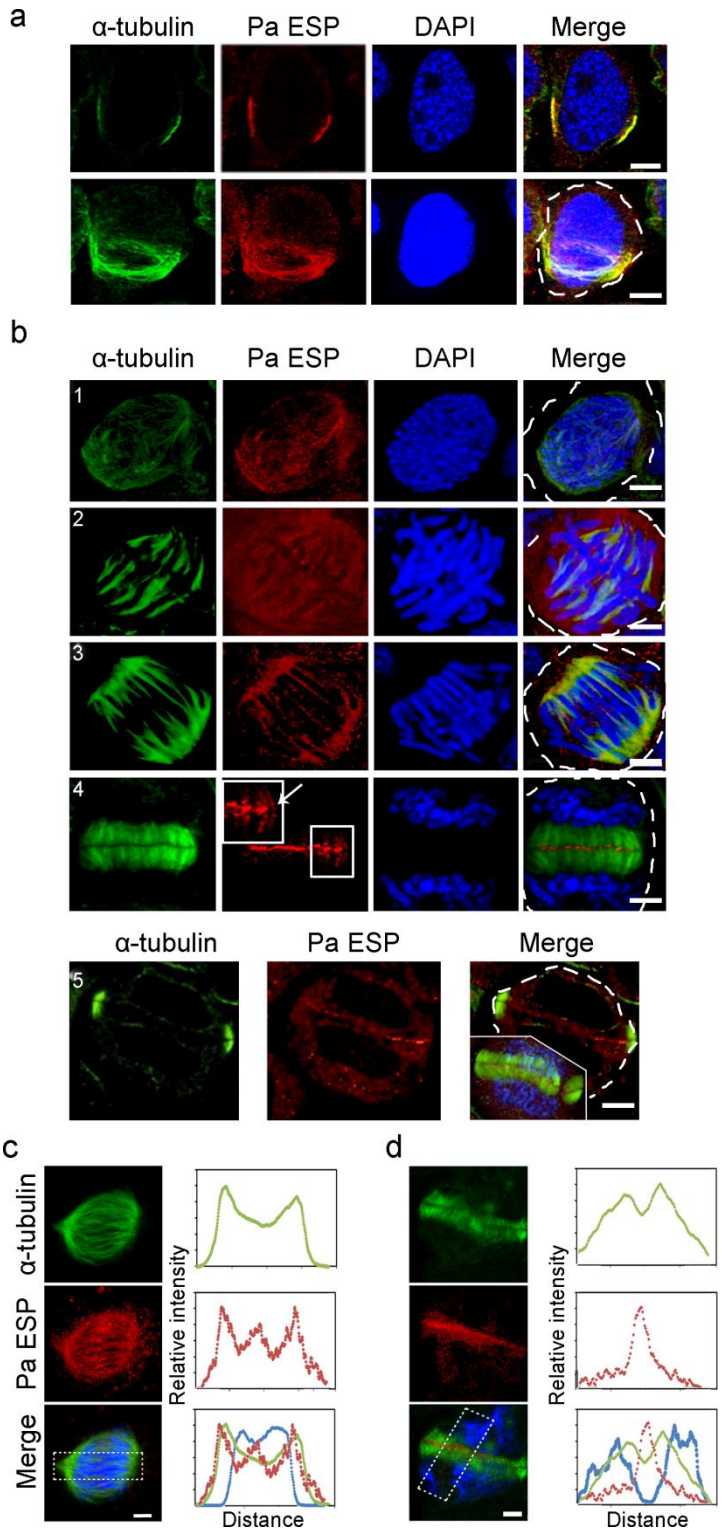
a
α-tubulin
Pa ESP
DAPI
Merge
b
α-tubulin
Pa ESP
DAPI
Merge
1
2
3
4
α-tubulin
Pa ESP
Merge
5
c
d
α-tubulin
Pa ESP
Merge
Relative intensity
Distance
Relative intensity
Distance

Fig. 3

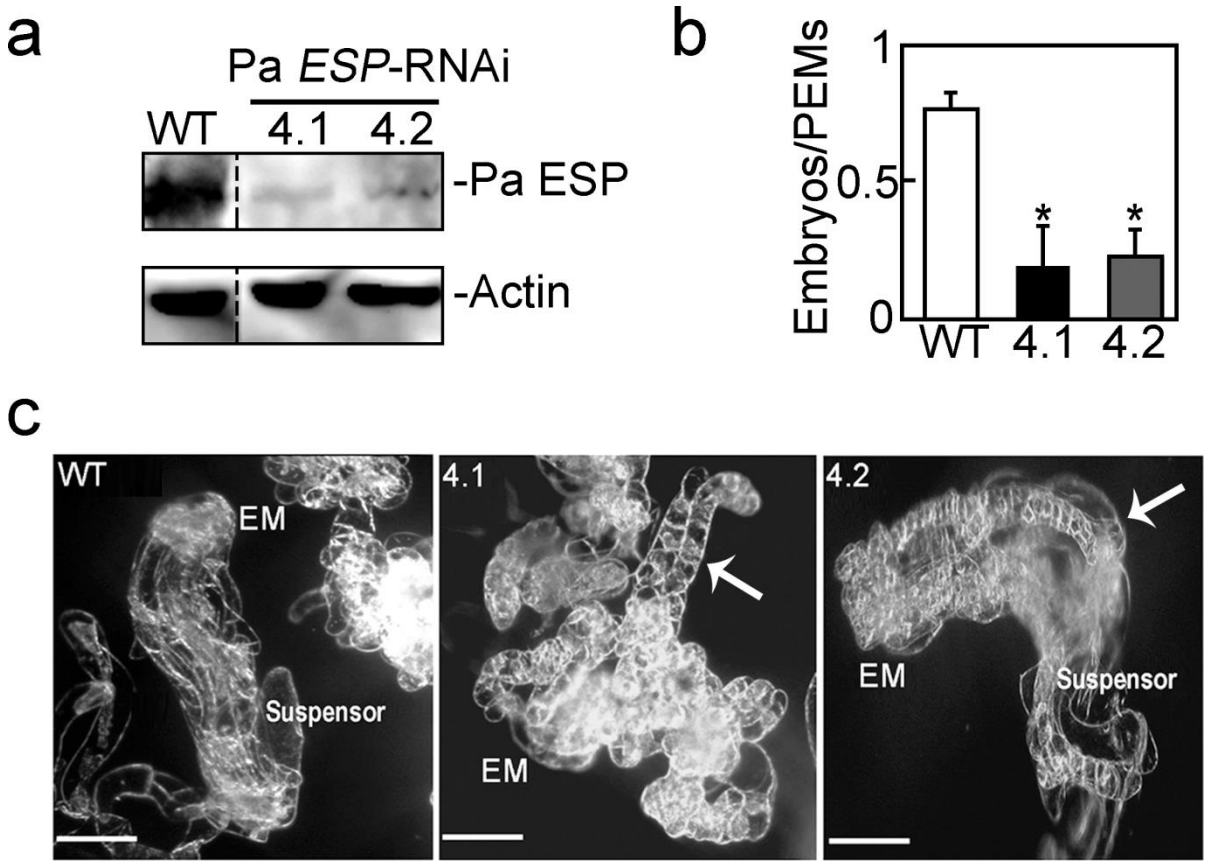

715
716 Fig. 4
717

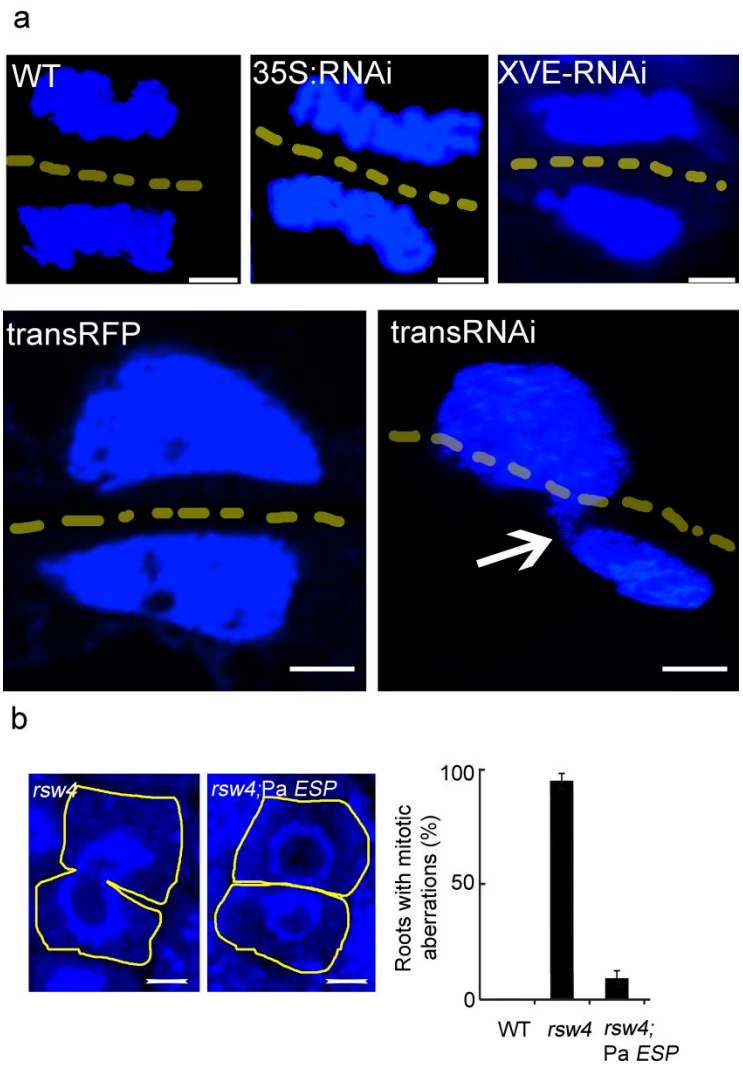

718
719 Fig. 5
720

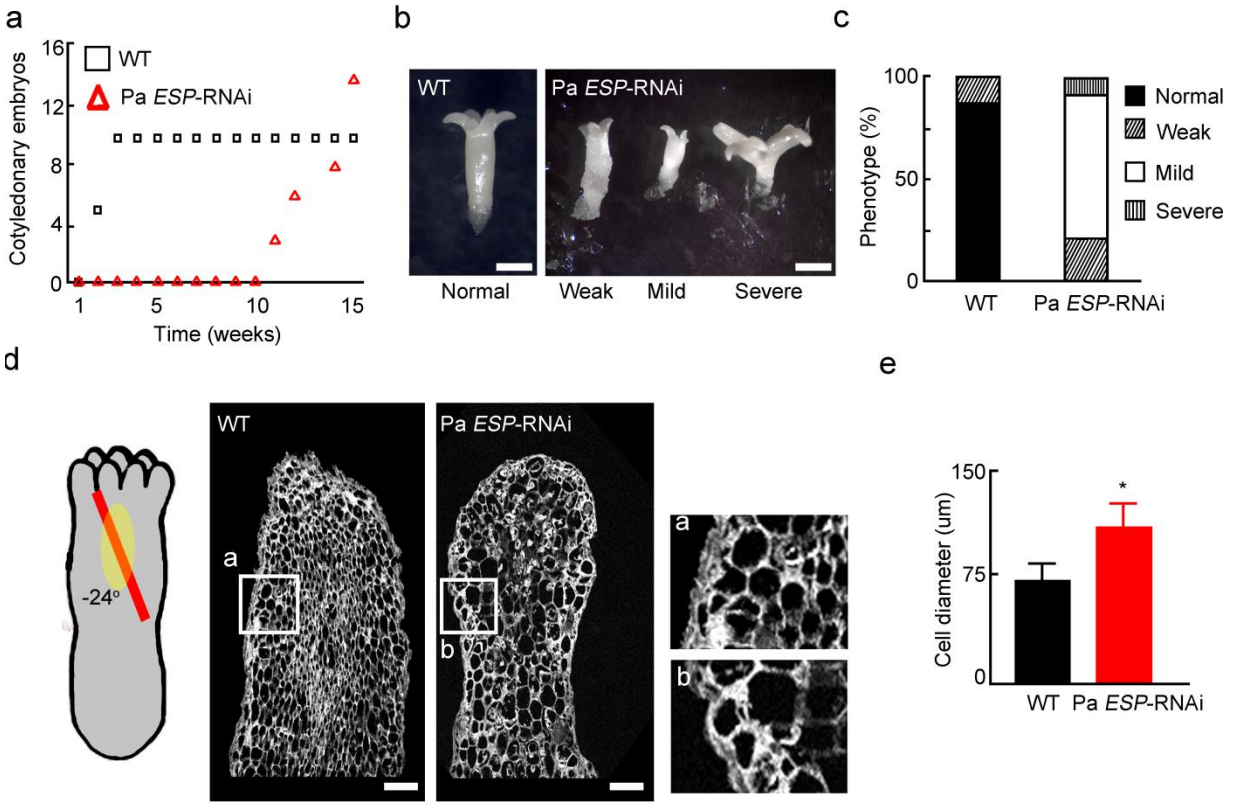

721
722 Fig. 6
723

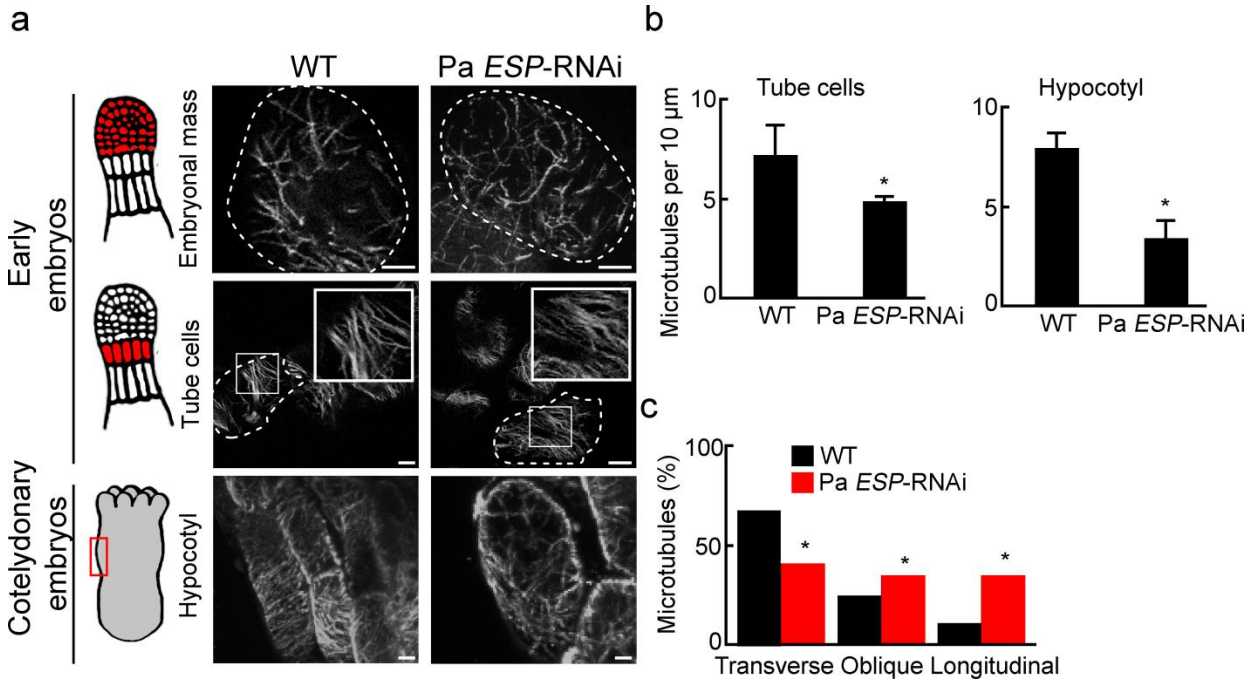
a
WT
Pa ESP-RNAi
Early embryos
Embryonal mass
Tube cells
Cotelydonary embryos
Hypocotyl
b
Tube cells
Hypocotyl
Microtubules per 10 µm
10
5
0
WT
Pa ESP-RNAi
c
Microtubules (%)
100
50
0
WT
Pa ESP-RNAi
Transverse Oblique Longitudinal

Fig. 7

727